Fuel 421 (2026) 139039

Contents lists available at ScienceDirect

Fuel

journal homepage: www.elsevier.com/locate/fuel

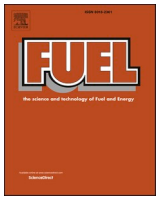

Full Length Article

Development of a novel fast screening method for fuel sooting tendency using soot precursor measurements in relation to the YSI☆

Jasmin Schmittner *, Nina Gaiser, Chiara Martyka, Thomas Bierkandt, Fabienne Werner, Joachim Schmid, Markus Köhler, Andreas Huber, Patrick Oßwald

Institute of Combustion Technology, German Aerospace Center (DLR), Stuttgart, Germany

ARTICLE INFO

Keywords:
YSI
SAF
Soot precursor
Molecular-beam mass spectrometry (MBMS)
Flow reactor
Derived sooting index (DSI)

ABSTRACT

Alternative aviation fuels are crucial to achieve CO_2 neutrality and reduce non-CO_2 climate effects. By reducing soot and advancing the understanding of contrail formation, these fuels hold the potential to mitigate warming effects on a global scale while also improving local air quality. Consequently, a comprehensive understanding of pollutant formation during the combustion of fuels or single component model fuels, with a particular focus on soot formation, is crucial for further fuel optimization. The development of fast and efficient methods for measuring parameters like the soot potential with regard to different molecular components are essential to achieve this objective. A novel screening method is currently under development to provide a fast overview of soot tendencies of different fuels or fuel components. To enhance the efficiency of measuring the soot tendency related to the yield sooting index (YSI), through the reduction of sample volumes, automation, and increased throughput in a shorter time frame compared to existing experiments with diffusion flames. This approach is based on measurements of soot precursors in the DLR's flow reactor coupled with molecular-beam mass spectrometry (MBMS). In order to optimize the throughput of samples, a standalone autosampler apparatus has been integrated into the existing experimental setup, together with a new method for the data evaluation. This study provides insights into the soot formation by demonstrating a correlation between measured signal intensities of $C_{12}H_{10}$ as soot precursor, obtained through the developed method, and the YSI, while also introducing a novel sooting index, called derived sooting index (DSI).

1. Introduction

Alternative, sustainable fuels represent a significant contribution in the pursuit of CO_2 neutrality within the aviation sector. The application of these sustainable aviation fuels (SAFs) has the potential to improve air quality at the local level and mitigate the climate impact by two distinct effects: reducing effective CO_2 emissions by its sustainable feedstock and non-CO_2 effects [1] by reducing aviation induced contrail formation.

With regard to the impact of climate change, it is of greater consequence to examine the influence of non-CO_2 effects than to focus on CO_2 alone. In their study, Lee et al. [1] estimated radiative forcing values for CO_2 at 34.3 mW/m^2 and for non-CO_2 emissions at up to 114.8 mW/m^2 in the year 2018, emphasizing the relevance of investigations into non-CO_2 terms. This climate metric describes the changes of the earth's energy balance due to alterations in radiation from space caused by external drivers, such as the amount of particles in the atmosphere [2]. Radiative forcing classifies the influence of emissions on the climate change as positive (warming) or negative (cooling) contribution [1–3]. For example, soot particles contribute to warming with radiative forcing values at 0.94 mW/m^2, exerting a significant radiative effect [1]. When considering the overall impact of total emissions, the net result of all mentioned contributions is a warming effect [3].

The adverse effect of soot particles on the climate is attributed to their involvement in the formation of contrails. This process is initiated by the emission of water vapor, which subsequently condenses onto soot and other atmospheric particles [4]. The formation of water droplets on the particles surface is initiated until they freeze due to low temperatures at higher altitudes in the troposphere. Consequently, contrails consist out of hundreds of ice particles, which are responsible for numerous negative impacts such as positive radiative forcing with

☆ This article is part of a special issue entitled: 'MCS13' published in Fuel.

* Corresponding author at: German Aerospace Center (DLR), Pfaffenwaldring 38-40, 70569 Stuttgart, Germany.
E-mail address: jasmin.bachmann@dlr.de (J. Schmittner).

https://doi.org/10.1016/j.fuel.2026.139039
Received 30 October 2025; Received in revised form 24 February 2026; Accepted 4 March 2026
Available online 13 March 2026

values at 111.4 mW/m^2 for high-humidity regions [1]. In response, the aviation sector is aiming for sustainable solutions to reduce these various emissions.

A significant contributing factor in the pursuit of CO_2 neutrality and the reduction of non-CO_2 effects within the aviation industry can also be achieved by alternative aviation fuels. The application of these fuels holds the potential to improve local air quality and mitigate the climate impact of aviation on a global scale once properly designed [5]. Voigt et al. [6] demonstrated that the formation of ice particles and the resulting contrails could be reduced by using alternative fuels compared to a conventional fossil reference fuel. Developing more environmentally friendly aviation fuels requires a deeper understanding of the formation pathways of pollutants during combustion processes and their dependence on the chemical composition of the fuel.

In this context, the formation mechanisms and mitigation of soot particles have become renewed significant areas of investigation in the field of emission research with major focus on the sooting tendency of different fuels. The tendency of a fuel to form soot is generally influenced by the chemical structures of the molecules [7–9]. Conventional jet fuels are complex mixtures composed of hundreds of individual compounds, encompassing a broad range of chemical structures and properties [10]. In both conventional and alternative aviation fuels, the main components are hydrocarbons with carbon chain lengths ranging from C8 to C16 [10]. The sooting tendency increases with the complexity of the molecules, and therefore, aromatic or polyaromatic structures have a strong influence on the soot nucleation process, leading to higher soot production [8,9]. Therefore, the hydrocarbon structures are the main focus of the evaluation of the fuel's sooting tendency.

During the combustion process, the fuel is degraded into hydrocarbon radicals and combustion intermediates. In the subsequent reaction stages, these radicals combine to form larger molecules, ultimately leading to the presence of polycyclic aromatic hydrocarbons (PAHs), which are known as soot precursor species. After the formation of soot precursors, the transition into the particle zone occurs along with surface growth. Through coagulation the soot particles are built up [11,12].

To quantitatively characterize the tendency of a fuel to form such particles, various sooting indices have been developed. The smoke point (SP) is a widely used parameter for evaluating the sooting behavior. It represents the flame height of a laminar wick flame at the onset of visible soot formation and is inversely related to the tendency of the respective sample to produce soot [13–16]. Lower SP values indicate stronger sooting tendencies. The exact procedure to measure this index can be found in the ASTM D1322.

In order to improve comparability across different instruments and laboratories, the threshold sooting index (TSI) was subsequently developed. This index converts measured SP into an instrument-independent metric based on calibration constants derived from reference compounds. In its equation, the molecular weight of the fuel is included to account for differences in the stoichiometric oxygen demand per mole of hydrocarbon, which is closely related to the carbon-to-hydrogen ratio of the respective sample and thus its intrinsic sooting tendency. By normalizing the SP with molecular weight, the TSI enables a more consistent comparison of sooting behavior among fuels of varying molecular structures [9,15–18].

Beyond the TSI, McEnally and Pfefferle [19] introduced an index without measurements of the SP to calculate the sooting tendency of different hydrocarbon structures and fuel mixtures doped into a base flame. The so-called yield sooting index (YSI) represents the basis for the method developed in this work and serves as a useful tool for the classification of single fuel components for their sooting potential. With this method the index can be calculated by the following equation according to [9]:

$$YSI_{TF} = (YSI_U - YSI_L) \times \frac{f_{TF} - f_L}{f_U - f_L} + YSI_L \quad (1)$$

where U and L describing the lower and the upper endpoint compounds to define a scale for the index. This indicates that YSI_U and YSI_L establish the evaluation scale, typically defined by toluene ($YSI_U = 170.9$) and n-heptane ($YSI_L = 36.0$). TF represents the equivalent test fuel being analyzed. The maximum soot volume fraction f_i of the different hydrocarbons is measured in the basic method by laser-induced incandescence (LII) at a co-flow non-premixed methane flame doped with the respective fuel of interest [19]. The resulting scale can be customized for various single components investigations by individually selecting the starting and ending points with specific parameters [9,19,20]. In the further development of this index, Das et al. [21] established a unified scale for neat compounds, with the objective of integrating disparate databases. This unified scale is specifically designed to facilitate the calculation of scales for oxygenated hydrocarbons, which are of greater relevance for biofuels. Herein, all YSIs refer to this unified scale.

The development of this index has led to the improvement of measurement methods for obtaining f_i. By using the experimental methods of color-ratio pyrometry, LII and laser extinction (LE) for measurements of f_i, it was possible to create a database with more than 400 hydrocarbon compounds on a unified scale [9,21,22]. The new scale grouped both non-aromatic and oxygenated compounds in YSI values between 6.6 and 161, while the YSIs of aromatic hydrocarbons span the range from 100 to 1400 [21]. An additional part of this study was the development of a model which predicts the YSI based on the molecular structure applying a group contribution model [9,21]. With the unified scale for different YSIs and the predicting model, a large scale with many hydrocarbons could be defined.

The study presented in this paper demonstrates that correlating YSI data with specific soot precursor species formed during the oxidation in a flow reactor setup of neat components, mixtures and complex fuels provides a valuable tool for screening the sooting tendency. This approach builds upon established constant temperature ramp measurement techniques, originally developed at DLR, which have traditionally been used to gain detailed insight into the kinetics of intermediate species formation, but are limited by long measurement times and high sample consumption [23–28]. By integrating key experimental principles of the constant ramp methodology into a fast, automated injection strategy, this approach represents a direct advancement of the conventional technique. It enables comparable chemical insight while significantly improving time efficiency through higher sample throughput and reduced required sample volumes (~2 mL). Above all, this development extends the capabilities of the experimental framework by enabling an efficient measurement of fuel sooting tendencies. This constitutes the central objective and primary contribution of this study. Based on this, the method offers the possibility to investigate soot precursor formation in the combustion processes of various fuels and single fuel components. However, the method is currently only applicable to fuels with low concentrations of multi-ring species or low aromatic fractions, as determining the sooting tendency of fuels with high fractions of either remains challenging. Regardless of this constraint, the analysis was intentionally restricted to samples with YSI values above 100, as this range is particularly relevant for the investigation of complex fuel compositions and soot formation in general. The prediction of the sooting tendency of different hydrocarbon structures is demonstrated by quantifying and comparing specific soot precursor molecules formed during the combustion process and subsequent calculation of a new sooting index called derived sooting index (DSI). This approach aims for the categorization of the sooting tendency of the respective fuel or neat component under investigation on a defined scale. Note, that the presented approach establishes the correlation earlier in the soot formation process compared to standard YSI measurement techniques, which primarily focus on soot particles. The investigation of the YSI correlation is therefore carried out with the soot precursor $C_{12}H_{10}$ by analyzing these species in an atmospheric flow reactor with electron-ionization molecular-beam mass spectrometry (EI-MBMS) at a defined temperature [23,24]. This soot precursor was

identified as a promising candidate through analyzing a previous study [24]. The selection of the soot precursor $C_{12}H_{10}$ was based on an evaluation of complex fuel measurement data from previous constant ramp experiments reported by Oßwald et al. [24], reanalyzed in accordance with the data treatment required for the DSI approach and afterwards measured again with the new developed approach. Among several soot precursors considered, $C_{12}H_{10}$ exhibited the strongest correlation with predicted YSI values and was therefore chosen for the present study. In the following, the experimental setup, the results containing preliminary experiments and their correlation with the YSI as well as its discussion will be demonstrated.

2. Experiment and investigated fuels

The experimental setup for the developed method consists of three main components: (1) an automated sample inlet system, (2) a flow reactor, and (3) an analytical data acquisition system. Fig. 1 illustrates the experimental setup of the flow reactor coupled with the automated sample application, the flow reactor and the EI-MBMS system including a time-of-flight (TOF) mass spectrometer [23].

The liquid samples are automatically injected with a 100-µL syringe (Smart syringe, U100-PrS-072-017-65LC) via an autosampler system (MultiPurposeSampler, GERSTEL). The autosampler system is implemented in the experimental setup and enables an automated sample preparation, application and cleaning process of the syringe. Reaction conditions are inspired by previous studies performed with this system [23–25]. After passing a heated injection port integrated in the autosampler system, the defined sample volume enters a carrier gas stream heated through heating hoses. To ensure complete evaporation for all samples this injection port is heated between 100 °C (373 K) up to 250 °C (523 K) depending on the boiling point of the respective sample using a heating tape. Following evaporation, the gas stream composes, besides the sample, of 17.64 g/min argon and 71.37 mg/min oxygen as the oxidizer. The flow rates of the gases are regulated by Coriolis mass flow controllers (Bronkhorst® mini CORI-FLOW). Flow conditions are carefully stabilized across all measurements, maintaining a constant fuel equivalence ratio of $\phi = 2$. The fuel flow is adjusted to the fixed oxygen flow to realize an injection period of 50 s at the desired equivalence ratio. Density at 20 °C (293 K) was applied to calculate the liquid volume flow. The residence time in the oven section of the reactor is dependent on the selected temperature. At 477 °C (750 K), the residence time is 2.8 s, whereas at 977 °C (1250 K), it decreases to 1.7 s.

The gas flux is preheated to 200 °C (473 K) after the injection process with heating hoses and transferred to the inlet flange of the flow reactor. The sample is highly diluted with more than 99% of the inert gas argon before entering the flow reactor in the next step to prevent heat release and self-sustaining reactions in the subsequent process.

The atmospheric flow reactor consists of a quartz tube with an inner diameter of 40 mm and a length of 1500 mm that is gas-tight mounted in a stainless-steel flange at the inlet. The temperature of the inlet flange is maintained at 200 °C using a heating tape. The flow reactor can be operated either with a controlled temperature ramp (e.g. 200 K/h), as used in previous detailed fuel investigations [23]. For this reference method, continuous fuel flow conditions are maintained by a commercial vaporizer (Bronkhorst® CEM W-102A-133-K) as used in previous studies [26,27,29]. Alternatively, the reactor can be held at a specific temperature in the new method, further mentioned as measurements for the derived sooting index (DSI). The reactor temperature in the experiments for this study vary from 700 to 900 °C (973–1173 K) in 50 K steps by a split tube furnace with a heated length of 1040 mm (Carbolite Gero model FZS 13/40/1000). The temperature difference between the reactor's inlet flange and the active heating zone generates a temperature profile along the reactor length, which is published in [25].

For analyzing, a gas sample is directly extracted from the reactive zone at the reactor outlet using a quartz nozzle. After passing the nozzle the products and intermediates from the combustion process undergo a two-stage expansion into the ionization chamber of the reflectron time-of-flight mass spectrometer (Kaesdorf, m/Δm = 3000 at m/z 28) to determine the exact elemental composition (C/H/O). Due to the significant pressure drop from atmospheric level to about 10^{-3}–10^{-4} mbar, a molecular-beam is formed, and the composition at the sampling position is preserved so that all chemical reactions are immediately quenched. The ionization process takes place at a two-stage Wiley-McLaren ion source. The nominal ionization energy is set to 13.5 eV (FWHM ≈ 1.4 eV), which is an adequate tradeoff between a sufficient signal intensity and low fragmentation. A detailed description of the applied EI-MBMS setup and the data acquisition process can also be found in [23].

The EI-TOF-MBMS system allows the analysis of different formed soot precursors at defined temperatures for each sample. The data acquisition process is synchronized with the injection method, commencing at the initiation of the autosampler injection method and ending at a point that exceeds the end of injection for a suitable time, described below in chapter 3.1, to capture the full process. The autosampler injection sequence itself begins with different wash steps with solvents for cleaning the syringe prior to the injection of the actual

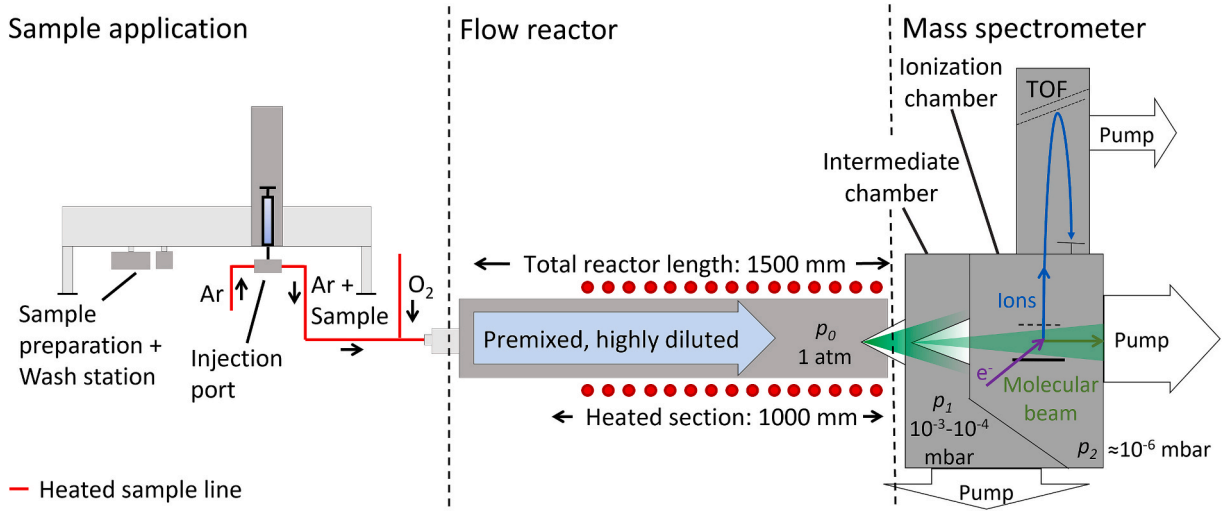

Fig. 1. Schematic figure of the automated sample application via autosampler, the flow reactor and the electron-ionization molecular-beam mass spectrometry (EI-MBMS) system including the time-of-flight (TOF) mass spectrometer.

sample.

2.1. Reference substances and fuels

A total of 16 different neat hydrocarbon samples as well as seven binary mixtures and nine different complex fuels are selected to analyze the soot precursor signals in correlation with YSI values. As the primary focus is on conventional and alternative jet fuels the selection is limited to neat hydrocarbons exhibiting YSI values above 100. Within this regime the selection represents a broad range of boiling points and YSI values. To access a continues YSI scale at the relevant range, binary mixtures were introduced. For this purpose, a low-sooting hydrocarbon, dodecane (YSI = 67.1), was combined with a higher-sooting aromatic compound, propylbenzene (YSI = 235.7). Both species are common representatives at technical jet fuels [24,30,31]. Table 1 shows the different samples and the YSI values from the unified scale [21] for the neat hydrocarbons. The YSI values for the mixtures were calculated by weighting the indices from literature with respective mole fractions.

A broad range of alternative and conventional complex fuels was selected, including conventional Jet A-1, hydrotreated Jet A-1, SAF blends containing Fischer–Tropsch (FT) fuel and hydroprocessed esters and fatty acids (HEFA) components, a catalytic hydrothermolysis jet (CHJ) fuel, as well as a high-aromatic surrogate. The technical fuels were gathered from a previously conducted speciation study [24] and combined with predicted YSI values. These predicted sooting indices were obtained from a model-based approach that estimates YSI values using the compositional group-type analysis assuming a uniform isomer distribution for available data at each chemical group. This model follows a weighted averaging method [32,33] and is reported on by Pütz et al. [34]. Reaction conditions are designed according similar to the neat substances, i.e., constant oxygen while maintaining the fuel flow to match the $\phi = 2$ conditions. Calculations are based on the reported bulk parameter (mean molar mass and C/H ratio) from [24]. An overview is given in Table 1.

3. Results and discussion

To gain a comprehensive understanding of the new measurement process, the injection system was examined for potential inconsistencies in terms of sample flow and data reproducibility. Additionally, the comparability between the constant ramp measurement procedure as reference and the new DSI-method was assessed in terms of temperature alignment. Using the soot precursor $C_{12}H_{10}$, an attempt was made to identify correlations between soot precursor species and existing YSI data.

3.1. Validation and verification of the experimental approach

To evaluate stability and consistency during sample injection, the automated sampling system was configured to deliver a steady fuel flow for a 50 s period to the flow reactor for the respective sample. The mass spectrometer was set to record one spectrum every seven seconds, resulting in a total of seven spectra over the 50 s injection period of the sample, enabling assessment of flow stability across the entire injection window. For these experiments, the reactor temperature was maintained at 200 °C (473 K) to prevent combustion reactions, focusing the mass spectra on fuel specific components.

Fig. 2 shows the results for three representative samples, benzene, 1-methylnaphthalene and diphenylmethane, representing species with intermediate and high boiling point, respectively. The signal intensity (a.u.) over the injection period displays a near-rectangular profile, indicating stable conditions within the reactor throughout the sample application.

Table 1
Investigated samples, including single components, binary dodecane/propylbenzene mixtures with their respective mole fractions of dodecane, and real fuel samples. The table lists the (average) molecular formula, YSI values from literature for the single components, calculated YSI values for the binary mixtures, predicted YSI values for the real fuels, and the injected fuel flux over 50 s [21,24].

Sample	Molecular formula	YSI	Injection flux [µL/s]
Dodecane	$C_{12}H_{26}$	67.1	0.93
Benzene	C_6H_6	100.3	0.88
Decahydronaphthalene	$C_{10}H_{18}$	105.5	0.81
Farnesane	$C1_5H_{32}$	109.8	0.89
1,8-Cineole	$C_{10}H_{18}O$	111.0	0.89
Bicyclohexyl	$C_{12}H_{22}$	117.1	0.82
R-Limonene	$C_{10}H_{16}$	137.4	0.86
Ethylbenzene	C_8H_{10}	216.0	0.86
Propylbenzene	C_9H_{12}	235.7	0.87
Butylbenzene	$C_{10}H_{14}$	245.1	0.86
Octylbenzene	$C_{14}H_{22}$	257.1	0.85
1,3,5-Trimethylbenzene	C_9H_{12}	310.9	0.86
1,2,3,4-Tetrahydronaphthalene	$C_{10}H_{12}$	336.0	0.78
1,5-Dimethyltetralin	$C_{12}H_{16}$	607.3	0.78
Diphenylmethane	$C_{13}H_{12}$	612.5	0.77
1-Methylnaphthalene	$C_{11}H_{10}$	649.1	0.77
Mixture YSI-79	$C_{11.7}H_{24.6}$ ($x_{C12} = 0.9$)	79.1	0.93
Mixture YSI-91	$C_{11.4}H_{23.2}$ ($x_{C12} = 0.8$)	91.9	0.92
Mixture YSI-105	$C_{11.1}H_{21.8}$ ($x_{C12} = 0.7$)	105.5	0.91
Mixture YSI-135	$C_{10.5}H_{19.0}$ ($x_{C12} = 0.5$)	135.9	0.90
Mixture YSI-171	$C_{9,9}H_{15.2}$ ($x_{C12} = 0.3$)	171.1	0.89
Mixture YSI-190	$C_{9,6}H_{14.8}$ ($x_{C12} = 0.2$)	190.8	0.88
Mixture YSI-212	$C_{9,3}H_{13.4}$ ($x_{C12} = 0.1$)	212.3	0.87
JS-A1.3	$C_{11.11}H_{22.31}$	100.2	0.88
E2-SAJF2	$C_{10.42}H_{21.05}$	111.9	0.89
E1-FSJF	$C_{11.36}H_{22.35}$	118.6	0.86
E1-SSJF1	$C_{16.26}H_{32.50}$	120.2	0.88
JS-A1	$C_{11.15}H_{21.67}$	135.9	0.88
E1-Ref2	$C_{11.85}H_{22.49}$	149.2	0.87
E2-Ref3	$C_{11.88}H_{22.38}$	157.7	0.86
JS-B3	$C_{11.43}H_{21.20}$	163.3	0.88
JS-C3	$C_{13.36}H_{24.01}$	207.1	0.85

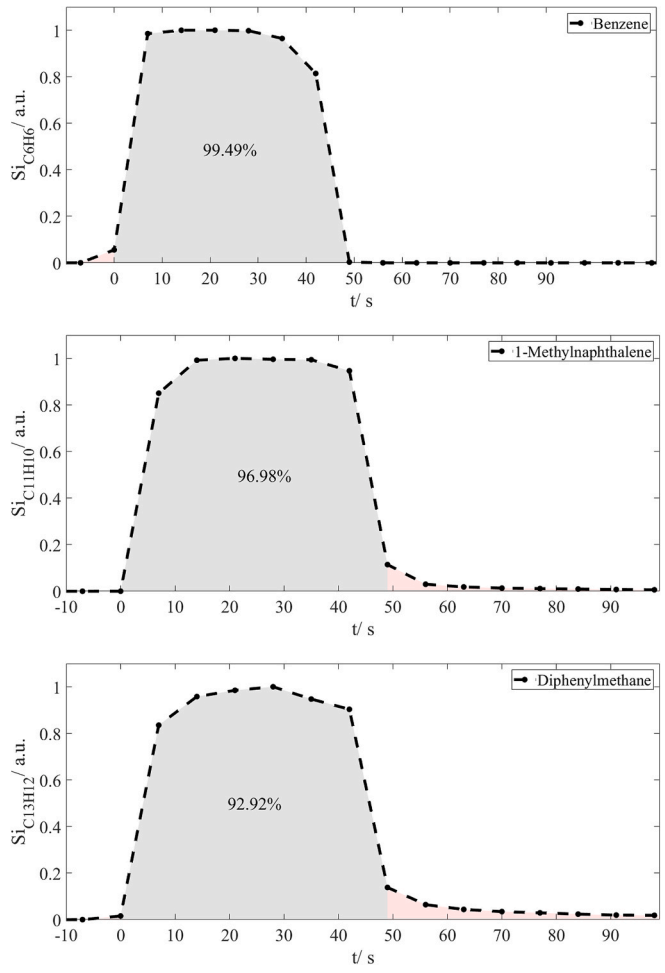

Fig. 2. Evaluation of the signal (a.u.) during the injection for the three exemplary samples benzene, 1-methylnaphthalene and diphenylmethane at 200 °C (473 K) with constant injection flow over 50 s and signal fraction within the predefined injection window (gray shape).

This near-rectangular shape, with a consistent signal level confirms that the automated injection system, equipped with the autosampler, delivers a steady and controlled sample flow.

The red-marked area at the end of the almost rectangular profile represents deviations caused by a trailing in the injection, which results from delayed vaporization of the respective compounds. 1-methylnaphthalene, with a boiling point of 245 °C (518 K), exhibits a higher retained fraction and a shorter tail compared to diphenylmethane, which has an even higher boiling point of 264 °C (537 K). Deviations of up to 10% were identified as the most critical case; thus, an approximately rectangular profile with more than 90% is considered acceptable. The stability of these profiles validates that the calculated measurement conditions were maintained for 50 s, with no observable shift in parameters like the fuel equivalence ratio. Ramp up and decay periods are expected to be negligible compared to the steady state period. This experiment was additionally performed for all other samples mentioned in chapter 2 with the similar results.

The reproducibility of the injection system combined with the MBMS setup was evaluated by performing three replicate measurements of the selected samples with YSI values over 100 at 800 °C (1073 K). Fig. 3 shows the mean relative signal of the soot precursor $C_{12}H_{10}$, with error bars representing the absolute standard deviation (1σ). The deviations were found to be negligible, with a maximum standard deviation of 0.05 (5.7% for 1,5-dimethyltetralin) and a minimum of 0.0007 (1.7% for benzene). These results confirm the reproducibility of the system,

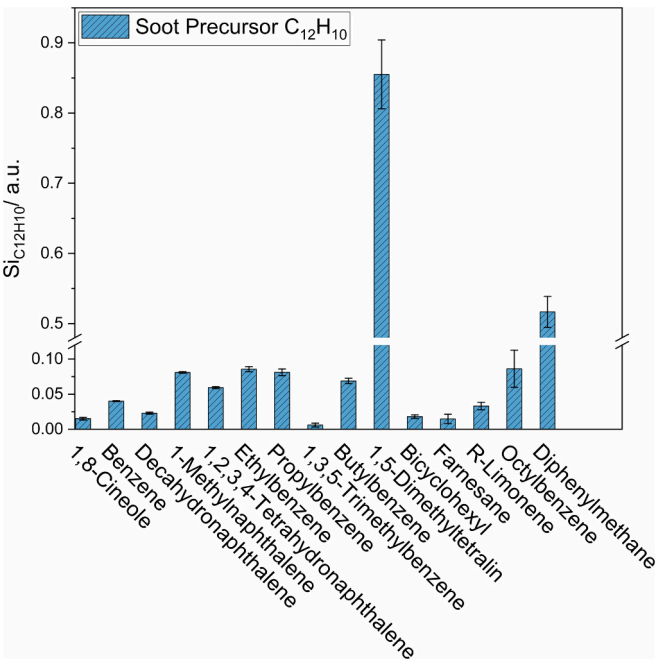

Fig. 3. Relative signal of the soot precursor $C_{12}H_{10}$ from the MBMS system for the neat hydrocarbon structures at 800 °C (1073 K) with error bars (one standard deviation of three measurements) from triple determination in full scale.

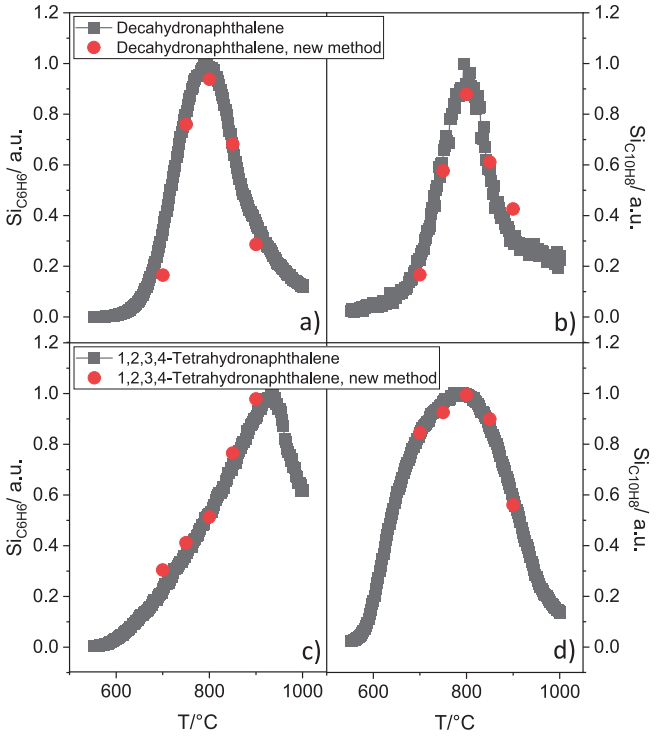

Fig. 4. Signal intensities of C_6H_6 (a and c) and $C_{10}H_8$ (b and d) from constant ramp measurements (grey) as well as the new methods (red) correlated to the temperature of the flow reactor for the samples decahydronaphthalene (a and b) and 1,2,3,4-tetrahydronaphthalene (c and d). (For interpretation of the references to colour in this figure legend, the reader is referred to the web version of this article.)

consequently, measurements at other temperatures were conducted only once.

Following the successful demonstration of stability and

reproducibility in the automated measurement system, a comparative analysis with the constant ramp measurements was conducted to evaluate data consistency. The DSI approach is based on the experimental framework of the constant temperature ramp measurements, utilizing the same flow reactor and MBMS system but incorporating a fast, automated injection strategy. This configuration enables more efficient measurements with reduced sample volumes while retaining the capability to investigate soot precursor formation and sooting tendencies. This comparison aimed to determine whether data acquired with the new DSI-method could be integrated with existing datasets to expand the overall database and build a more comprehensive basis for analysis. 16 neat components were measured with the DSI-method for reactor temperatures spanning from 700 °C (973 K) to 900 °C (1173 K) in 50 K steps to gain respective temperature profiles. Intermediate species evolution with the reactor temperature can be reconstructed from those five injections. For reference, data from the constant ramp measurement procedure was obtained using decahydronaphthalene (decalin) and 1,2,3,4-tetrahydronaphthalene (tetralin) as test samples.

In the constant ramp measurements, the temperature ranged from 550 °C (823 K) to 1000 °C (1273 K), with a controlled temperature decrease of 200 K/h. Fig. 4 compares normalized soot precursor responses of C_6H_6 (a and c) and $C_{10}H_8$ (b and d), obtained from both methods for the fuels decahydronaphthalene and 1,2,3,4-tetrahydronaphthalene. Dataset from both measurement techniques were acquired under rich fuel conditions ($\phi = 2$) allowing a direct comparison. The signal intensity profiles as a function of temperature reveal that the peak positions of both investigated soot precursors align closely across both methods.

This proves the ability of reconstruction the well-known species evolution of fuels and single components [28,35] by single injections at selected temperatures. As a result, the two measurement approaches are comparable in terms of soot precursor generation relative to temperature. The comparability of the two methods validates that previously acquired data can be compared to data from the new DSI-method, facilitating an expanded dataset and enabling broader analysis of soot formation dynamics. Note that under these conditions, the peak concentrations of most soot precursors occur between 800 °C (1073 K) and 950 °C (1173 K), which enables further correlation of the YSI with soot precursor signals. A set of five temperatures, i.e., 700, 750, 800, 850 and 900 °C, has been identified to cover the majority of soot precursors within the selected fuels.

3.2. Soot precursor selection for the DSI-method

Previous studies, e.g. [16,36,37] have proven the ability of rating a specific sooting propensity of complex fuels and single compounds. In order to determine a suited soot precursor, species for particular ranking technical fuels, the respective peak mole fractions from previous detailed speciation study involving various complex jet fuels were correlated. In the study by Oßwald et al., 42 jet fuels were investigated [24] and nine of them were selected for the present work based on their availability and the ability of predicting YSI data. Fig. 5 presents the peak maximum signal obtained from constant ramp measurements of the soot precursors $C_{12}H_{10}$ (c), C_6H_6 (a) and $C_{13}H_{10}$ (b) for these nine

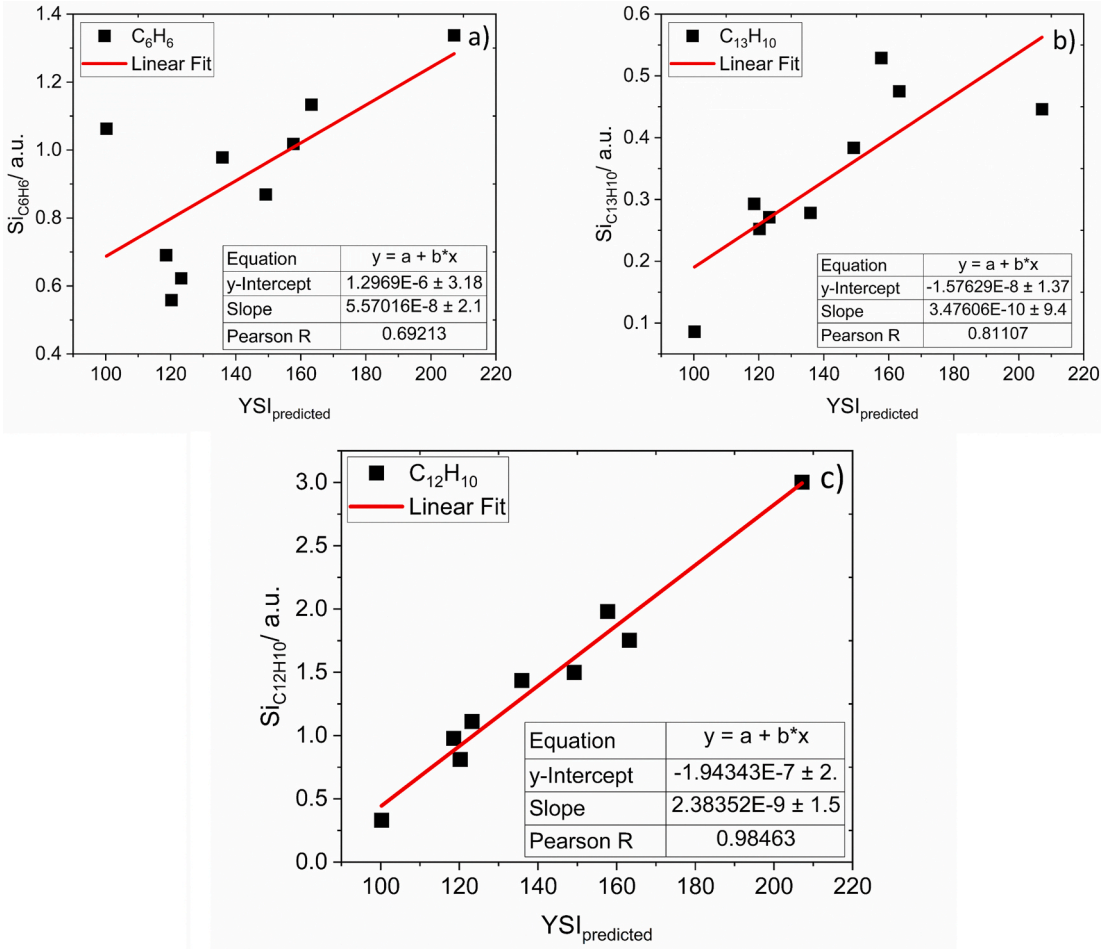

Fig. 5. Correlation between peak mole fraction of the soot precursors C_6H_6 (a), $C_{13}H_{10}$ (b) and $C_{12}H_{10}$ (c) for the jet fuels gathered from constant ramp measurements at the MBMS setup [24] and predicted YSI values based on the molecular composition of the complex fuels; Linear fit in red. (For interpretation of the references to colour in this figure legend, the reader is referred to the web version of this article.)

fuels, correlated with their predicted YSI values. The strongest correlation to YSI was found for the soot precursor signal of $C_{12}H_{10}$ (c), confirmed by a linear fit (red line), yielding a Pearson R of 0.98. Weaker correlations are seen for smaller (e.g. benzene, C_6H_6) as well as larger soot precursor species (e.g. $C_{13}H_{10}$, expected to consist primarily from fluorene).

Non ideal correlation of small soot precursors as benzene or substituted benzenes for the jet fuels can be expected since these fuels typically consist of a noticeable fraction of aromatic compounds, primarily substituted benzenes. For technical fuels containing aromatics, previous studies have not validated benzene as proper predictor of its sooting propensity when particular direct reaction channels from

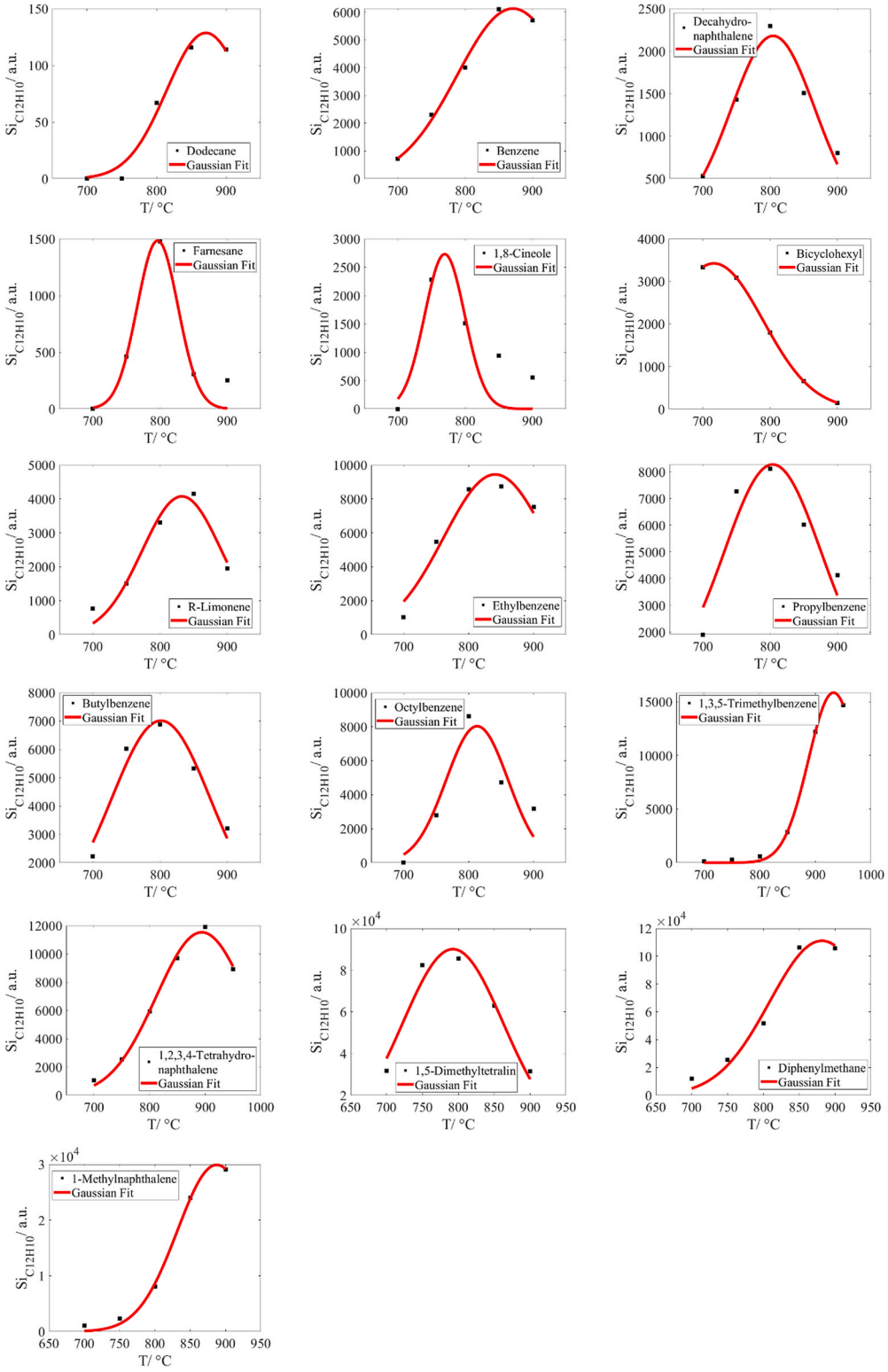

Fig. 6. Signals of the soot precursor $C_{12}H_{10}$ obtained from the new injection system combined with MBMS system across all investigated temperatures for 16 neat hydrocarbon structures; Peaks interpolated with a Gaussian fit (red line). (For interpretation of the references to colour in this figure legend, the reader is referred to the web version of this article.)

specific fuel constituents towards benzene are active [16,24]. From this perspective a large soot precursor should be chosen to ensure equilibration of individual fuel specific reaction channels. However, larger soot precursor species decrease in concentration and approach the detection limit of the measurement system. Pyrene isomers ($C_{16}H_{10}$) for example have only been detected for very high sooting fuels. $C_{13}H_{10}$ appears to be the largest precursor exhibiting a sufficient signal-to-noise ratio for all fuels even though scatter is clearly increased compared to $C_{12}H_{10}$. For this reason, the soot precursor $C_{12}H_{10}$ was selected in the following. Please note that for the elemental composition $C_{12}H_{10}$, the isomers acenaphthene with its naphthalene base structure as well as biphenyl with its benzene base structure have to be expected to contribute to signal and different formation routes may exhibit still over proportional sensitivity to specific fuel components. To assess potential contributions from different formation pathways and isomer-specific fragmentation behavior, the fragmentation patterns of acenaphthene and biphenyl were investigated at 200 °C under the applied experimental conditions; the corresponding mass spectra are provided in the supplementary material (supporting Fig. S1). No observable fragmentation patterns were identified that could affect the subsequent correlations and slope determinations.

3.3. Species peak reconstruction and intensity determination

Due to the convincing correlation between YSI values and the peak mole fraction of $C_{12}H_{10}$ measured at the detailed jet fuel experiments [24] determination of the actual peak signal value appears appropriate. Actually, initial approaches at a fixed temperature had indeed not shown comparable correlation to the reference YSIs. Also considering the maximum signal from a set of temperatures is not fully convincing. For this reason, a peak signal determination strategy was developed with five specific temperatures, ranging from 700 °C (973 K) to 900 °C (1173 K), where the actual signal peak is determined based on a Gaussian fit.

For the samples 1,2,3,4-tetrahydronaphthalene and 1,3,5-trimethylbenzene, additional data points at 950 °C (1223 K) were included to improve the further fit process. This enables the replication of the results from the constant ramp measurements using only a limited number of data points at these defined temperatures. The uncertainty in the interpolated peak signal obtained using the Gaussian fit function is 18.3%. The Gaussian fit function is used to interpolate the peak maximum from at least five data points, aiming to reproduce the values obtained from the time-consuming constant ramp measurements, which typically require several hours. Fig. 6 presents the signals of the soot precursor $C_{12}H_{10}$ across all investigated temperatures for the 16 neat hydrocarbon structures, which were used as calibration samples for the subsequent determination of the complex fuels. The peak value of the Gaussian fit (red line) serves as the basis for further correlation analysis. Fig. 6 demonstrates that the peak maxima can be successfully interpolated from only a few data points, with the Gaussian fit sufficiently representing the measured values.

3.4. YSI correlation with the DSI-method

The following section presents data from the oxidation experiments conducted on 16 different neat samples, seven mixtures and nine different complex fuels using the flow reactor setup with the new DSI-method. For the investigation of the correlation between the YSI values of these samples and the mass spectrometer signals of the soot precursor $C_{12}H_{10}$, a temperature range between 700 °C (973 K) and 900 °C (1173 K) in 50 K steps was recorded and processed to interpolated the peak maxima. This correlation may serve as a calibration step for the subsequent analysis of complex fuel mixtures.

Fig. 7 presents the relationship between the peak soot precursor signals and the YSI values obtained from YSI database [21]. For 13 molecular structures, the linear fit (red line) demonstrates an acceptable correlation with a Pearson coefficient of 0.98. The 95% confidence interval (CI) including upper (UL) and lower limit (LL) were determined for both, the slope and the y-intercept of the regression. For the slope, the 95% confidence interval ranges from 43.8 (LL) to 57.1 (UL), while for the y-intercept the corresponding limits span from −5022.3 (LL) to −1456.5 (UL). Three outliers, 1,5-dimethyltetralin, benzene, and diphenylmethane, were identified and excluded from the fit. These species likely promote the direct formation of $C_{12}H_{10}$ through specific structural features. 1,5-dimethyltetralin already contains the carbon framework of acenaphthene and may form $C_{12}H_{10}$ through dehydrogenation, whereas benzene can generate phenyl radicals that recombine to form biphenyl. Diphenylmethane may thermally decompose to phenyl radicals, which can also recombine to yield $C_{12}H_{10}$ [38]. As a

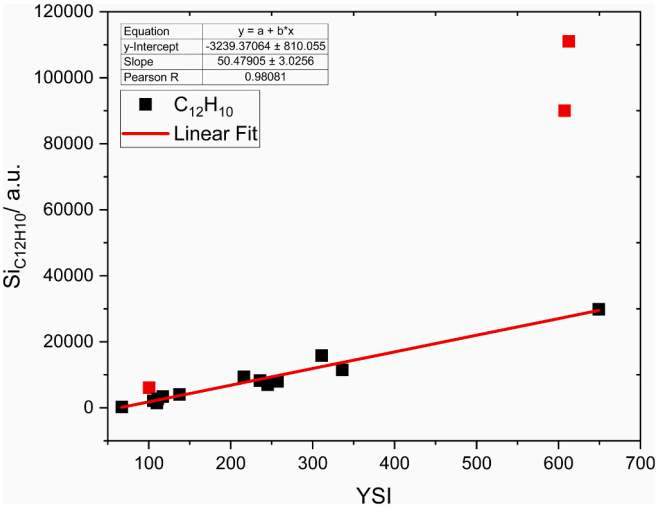

Fig. 7. Peak maximum signals of the soot precursor $C_{12}H_{10}$ obtained from the new injection system combined with MBMS for 16 neat hydrocarbon structures with outliers marked as red points (1,5-dimethyltetralin (YSI = 607.3), benzene (YSI = 100.3), and diphenylmethane (YSI = 612.5)); Linear fit as red line with 95% CI for slope (UL = 57.1, LL = 43.8) and y-intercept (UL = −1456.5, LL = -5022.3). (For interpretation of the references to colour in this figure legend, the reader is referred to the web version of this article.)

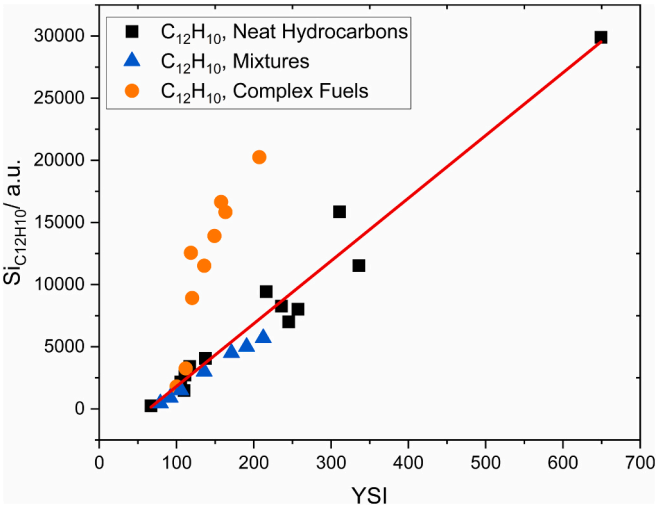

Fig. 8. Peak maximum signals of the soot precursor $C_{12}H_{10}$ obtained from the new injection system combined with MBMS for 16 neat hydrocarbon structures (black squares), seven mixtures (blue triangles) and nine complex fuels (orange dots). (For interpretation of the references to colour in this figure legend, the reader is referred to the web version of this article.)

result, these fuels produce disproportionately high $C_{12}H_{10}$ signals relative to their overall sooting tendency and are therefore not representative for the general correlation.

However, the focus of this study lies primarily on the YSI range between 100 and 300, which is most relevant for jet fuel samples in the further process and uncertainties at these higher YSIs may be acceptable.

In the next step, the measured signals of the soot precursor $C_{12}H_{10}$ were analyzed for the designed mixtures and the complex fuels. The peak maxima were again determined using a Gaussian fit based on these discrete temperature points. The results for all seven mixtures as well as the nine complex fuels are comparable to the data shown in Fig. 7 and provides a reliable estimation of the peak maximum of the soot precursor $C_{12}H_{10}$. Fig. 8 presents the relationships of peak maximum and respective YSI values across the different sample groups. The comparison reveals that the correlation for the neat hydrocarbons and the binary mixtures collapse and follow a similar trend. In contrast, the correlations for the complex fuels deviate noticeable from this trend, indicating that their behavior does not align with the aforementioned trend. This is unexpected facing the strong linearity within the fuel series. This behavior either hints toward a massive underestimation of the YSI by the modeling approach or the significant contribution of fuel species exhibiting direct reaction channels towards $C_{12}H_{10}$ as seen for some of the neat compounds. However, based on the measured signals the fuels would need to have YSIs up to 450 which appears to be unrealistic. As a consequence, we expect the multiring components (aromatic as well as aliphatic) forcing this over-proportional formation of $C_{12}H_{10}$ at the complex fuels only. Indeed, a collapse of the trends can be observed for lager soot precursor but a reliable correlation is prohibited by the low signal level.

Unfortunately, this behavior does not allow to determine DSI for jet fuels based on $C_{12}H_{10}$ and a significant increase of sensitivity is needed to reliably determine higher soot precursor species following the DSI logic yet. Nevertheless, the systematic approach of determining a DSI based on soot precursor species for ranking the sooting tendency of fuels can still be verified for fuels that do not exhibit larger cyclic fuel constituents, i.e., the tailored mixtures, while the determination of highly aromatic fuels remains a limitation. Another limitation of the presented correlation is the selected YSI range. Within the range considered in this study, the correlation is valid and reproducible. However, the correlation based on the soot precursor $C_{12}H_{10}$ cannot be extended to YSI values below 100. For neat hydrocarbons in this lower YSI regime, the targeted soot precursor cannot be detected with the applied MBMS setup, as such large soot precursors are not formed under the selected measurement conditions at low sooting tendencies. Consequently, the applicability of the correlation is currently restricted to the investigated YSI range. Despite these limitations, the method offers several advantages. These include a high degree of automation, enabling increased sample throughput while requiring only a small sample volume (~2 mL) and shorter measurement times.

Using the linear correlation established between the neat hydrocarbons and their YSI values, the DSI was calculated for the binary mixtures. Table 2 summarizes the calculated DSI values in comparison with the corresponding YSI values for the respective mixture. The results demonstrate that the newly developed DSI-method provides reliable predictions for mixtures and surrogates, as the DSI and YSI values agree closely within the experimental uncertainty. The comparatively larger uncertainties of the new method relative to the established YSI approach underline the need for further optimization, which is expected to benefit from improvements in signal intensities. However, the failure of determining a plausible DSI for the complex fuels discloses a significant restriction: The chosen soot precursor needs to be decoupled from direct fuel decomposition pathway, i.e., it needs to be significantly larger than the fuel constituent to ensure an equal distribution to the soot formation channels.

Table 2
Comparison of YSI data calculated from the mole fractions of the mixtures and calculated DSI values from signal intensities of the soot precursor $C_{12}H_{10}$ for all mixtures.

	YSI	DSI
Mixture YSI-79	79.1 ± 3.22	73.1 ± 22.63
Mixture YSI-91	91.9 ± 3.36	82.0 ± 23.19
Mixture YSI-105	105.5 ± 3.81	93.9 ± 23.94
Mixture YSI-135	135.9 ± 5.23	123.6 ± 25.84
Mixture YSI-171	171.1 ± 7.00	153.3 ± 27.77
Mixture YSI-190	190.8 ± 7.95	163.2 ± 28.42
Mixture YSI-212	212.3 ± 8.92	177.1 ± 29.33

4. Conclusion and outlook

This study presents the first results from a novel method for the assessment of the sooting potential of liquid fuel samples. A respective soot index, called derived sooting index (DSI), is established. The method allows for higher sample throughput, while requiring only a small sample volume, thereby enhancing efficiency and reducing material consumption. The established setup was expanded with an automated sample application system to ensure reproducibility and facilitate high-throughput operation. Comparability with previous measurement series at the flow reactor allows the integration of previous data, thereby enabling the transfer of established experimental findings to the new soot precursor-based method. Yale's YSI values were compared to soot precursor signals ($C_{12}H_{10}$) obtained during oxidation by molecular-beam mass spectrometry coupled to an atmospheric flow reactor. A good correlation between YSI and DSI was demonstrated for both single components and binary mixtures thus underscoring the functionality of the method. This is a proof of the functionality of the experimental setup and the process of the data handling and evaluation. The presented results principally demonstrate the ability of determining soot propensity of fuels based on comparison of intermediately formed soot precursors and their ranking by a respective index. Its application within as fuel screening and development process may enable efficient development of alternative sustainable fuels.

While major efforts have already been made, the next step is undoubtedly to cover complex technical fuel mixtures. Further research is required to establish a correlation between the soot precursor signals and the YSI values for complex fuels containing multiring compounds. First attempts indicate significant deviations from the behavior of the neat hydrocarbons and the binary mixtures that may overcome by the application of larger soot precursors species, but sensitivity of the system is not sufficient for proper evaluation of larger soot precursors yet. Further research is required to extend the DSI-method to larger complex fuels and to verifying the underlying detailed causes of their differing behavior compared to single components and binary mixtures. The largest uncertainty arises from the peak interpolation using the Gaussian fit function. However, this also presents an opportunity to improve the new method and reduce uncertainty by exploring alternative fit functions that could better interpolate and represent the data points. Once this integration is achieved, subsequent work should also address fuels and neat hydrocarbon structures with YSI values below 100 to better understand their sooting behavior within the framework of the new method.

CRediT authorship contribution statement

Jasmin Schmittner: Writing – original draft, Visualization, Validation, Methodology, Investigation, Formal analysis, Conceptualization. **Nina Gaiser:** Writing – review & editing, Supervision, Methodology. **Chiara Martyka:** Writing – review & editing, Investigation. **Thomas Bierkandt:** Writing – review & editing, Methodology, Investigation. **Fabienne Werner:** Writing – review & editing, Investigation. **Joachim Schmid:** Investigation. **Markus Köhler:** Writing – review & editing,

Supervision, Funding acquisition. **Andreas Huber:** Supervision. **Patrick Oßwald:** Writing – review & editing, Supervision, Methodology, Funding acquisition.

Declaration of competing interest

The authors declare that they have no known competing financial interests or personal relationships that could have appeared to influence the work reported in this paper.

Acknowledgments

The authors gratefully acknowledge funding by the German Federal Ministry for Digital and Transport (BMDV) within the M2SAF project (FKZ: 16RK14001A-E). The authors are grateful to Thomas “Manni” Mannsdörfer for the valuable support in preparing the measurements and for providing technical advice and guidance regarding the experimental setup.

Appendix A. Supplementary data

Supporting figures, raw data from the MBMS system and temperature profiles from the flow reactor are included in the supplementary material. Supplementary data to this article can be found online at https://doi.org/10.1016/j.fuel.2026.139039.

Data availability

Data will be made available on request.

References

[1] Lee DS, Fahey DW, Skowron A, Allen MR, Burkhardt U, Chen Q, et al. The contribution of global aviation to anthropogenic climate forcing for 2000 to 2018. Atmos Environ 2021;244:117834. https://doi.org/10.1016/j.atmosenv.2020.117834.
[2] Ramanswamy V, Shine K, Leovy C, Wang W-C, Rodhe H, Wuebbles DJ, Ding M, Lelieveld J, Edmonds JA, Mccormick MP. Radiative forcing of climate. NASA, Washington, Scientific Assessment of Ozone Depletion; 1991.
[3] Lee DS, Fahey DW, Forster PM, Newton PJ, Wit RCN, Lim LL, et al. Aviation and global climate change in the 21st century. Atmos Environ 2009;43(22):3520–37. https://doi.org/10.1016/j.atmosenv.2009.04.024.
[4] Kärcher B. Formation and radiative forcing of contrail cirrus. Nat Commun 2018;9(1):1824. https://doi.org/10.1038/s41467-018-04068-0.
[5] Schripp T, Anderson BE, Bauder U, Rauch B, Corbin JC, Smallwood GJ, et al. Aircraft engine particulate matter emissions from sustainable aviation fuels: results from ground-based measurements during the NASA/DLR campaign ECLIF2/ND-MAX. Fuel 2022;325:124764. https://doi.org/10.1016/j.fuel.2022.124764.
[6] Voigt; C, Kleine J, Sauer D, Moore RH, Bräuer T, Le Clercq P, et al. Cleaner burning aviation fuels can reduce contrail cloudiness. Commun Earth Environ 2021;2(1):114. https://doi.org/10.1038/s43247-021-00174-y.
[7] Frenklach M, Wang H. Detailed mechanism and modeling of soot particle formation. In: Bockhorn H, editor Soot Formation in Combustion: Mechanisms and Models. Berlin Heidelberg: Springer; 1994. https://doi.org/10.1007/978-3-642-85167-4_10.
[8] Glassman I. Soot formation in combustion processes. Symp (Int) Combust 1989;22(1):295–311. https://doi.org/10.1016/S0082-0784(89)80036-0.
[9] Pfefferle LD, Kim S, Kumar S, McEnally CS, Pérez-Soto R, Xiang Z, et al. Sooting tendencies: combustion science for designing sustainable fuels with improved properties. Proc Combust Inst 2024;40(1):105750. https://doi.org/10.1016/j.proci.2024.105750.
[10] Blakey S, Rye L, Wilson CW. Aviation gas turbine alternative fuels: a review. Proc Combust Inst 2011;33(2):2863–85. https://doi.org/10.1016/j.proci.2010.09.011.
[11] Bockhorn H, D'Anna A, Sarofim AF, Wang H. Combustion Generated Fine Carbonaceous Particles. Universitätsverlag Karlsruhe; 2009.
[12] Tree DR, Svensson KI. Soot processes in compression ignition engines. Prog Energy Combust Sci 2007;33(3):272–309. https://doi.org/10.1016/j.pecs.2006.03.002.
[13] Hunt RA. Relation of smoke point to molecular structure. Ind Eng Chem 1953;45(3):602–6. https://doi.org/10.1021/ie50519a039.
[14] Kent JH. A quantitative relationship between soot yield and smoke point measurements. Combust Flame 1986;63(3):349–58. https://doi.org/10.1016/0010-2180(86)90004-0.
[15] Watson RJ, Botero ML, Ness CJ, Morgan NM, Kraft M. An improved methodology for determining threshold sooting indices from smoke point lamps. Fuel 2013;111:120–30. https://doi.org/10.1016/j.fuel.2013.04.024.
[16] Zinsmeister J, Storch M, Melder J, Richter S, Gaiser N, Schlichting S, et al. Soot formation of renewable gasoline: from fuel chemistry to particulate emissions from engines. Fuel 2023;348:128109. https://doi.org/10.1016/j.fuel.2023.128109.
[17] Calcote HF, Manos DM. Effect of molecular structure on incipient soot formation. Combust Flame 1983;49(1):289–304. https://doi.org/10.1016/0010-2180(83)90172-4.
[18] Abdul Jameel AG. Predicting sooting propensity of oxygenated fuels using artificial neural networks. Processes 2021;9(6):1070. https://doi.org/10.3390/pr9061070.
[19] McEnally CS, Pfefferle LD. Improved sooting tendency measurements for aromatic hydrocarbons and their implications for naphthalene formation pathways. Combust Flame 2007;148(4):210–22. https://doi.org/10.1016/j.combustflame.2006.11.003.
[20] McEnally CS, Pfefferle LD. Sooting tendencies of nonvolatile aromatic hydrocarbons. Proc Combust Inst 2009;32(1):673–9. https://doi.org/10.1016/j.proci.2008.06.197.
[21] Das DD, St. John PC, McEnally CS, Kim S, Pfefferle LD. Measuring and predicting sooting tendencies of oxygenates, alkanes, alkenes, cycloalkanes, and aromatics on a unified scale. Combust Flame 2018;190:349–64. https://doi.org/10.1016/j.combustflame.2017.12.005.
[22] McEnally CS, Das DD, Pfefferle LD. Yield sooting index database volume 2: Sooting tendencies of a wide range of fuel compounds on a unified scale, harvard dataverse, v V1; 2017. doi: 10.7910/DVN/7HGFT8.
[23] Oßwald P, Köhler M. An atmospheric pressure high-temperature laminar flow reactor for investigation of combustion and related gas phase reaction systems. Rev Sci Instrum 2015;86(10). https://doi.org/10.1063/1.4932608.
[24] Oßwald P, Zinsmeister J, Kathrotia T, Alves-Fortunato M, Burger V, van der Westhuizen R, et al. Combustion kinetics of alternative jet fuels, Part-I: Experimental flow reactor study. Fuel 2021;302:120735. https://doi.org/10.1016/j.fuel.2021.120735.
[25] Bierkandt T, Gaiser N, Bachmann J, Oßwald P, Köhler M. Terpene speciation: Analytical insights into the oxidation and pyrolysis of limonene and 1,8-cineole via molecular-beam mass spectrometry. Combust Flame 2025;272:113854. https://doi.org/10.1016/j.combustflame.2024.113854.
[26] Werner F, Kathrotia T, Bierkandt T, Schmid J, Gaiser N, Bachmann J, et al. Oxidation of MTBE and ETBE at atmospheric and elevated pressure. Proc Combust Inst 2025;41:105863. https://doi.org/10.1016/j.proci.2025.105863.
[27] Gaiser N, Bierkandt T, Oßwald P, Zinsmeister J, Kathrotia T, Shaqiri S, et al. Oxidation of oxymethylene ether (OME0−5): an experimental systematic study by mass spectrometry and photoelectron photoion coincidence spectroscopy. Fuel 2022;313:122650. https://doi.org/10.1016/j.fuel.2021.122650.
[28] Zinsmeister J, Gaiser N, Melder J, Bierkandt T, Hemberger P, Kasper T, et al. On the diversity of fossil and alternative gasoline combustion chemistry: a comparative flow reactor study. Combust Flame 2022;243:111961. https://doi.org/10.1016/j.combustflame.2021.111961.
[29] Kathrotia T, Naumann C, Oßwald P, Köhler M, Riedel U. Kinetics of ethylene glycol: the first validated reaction scheme and first measurements of ignition delay times and speciation data. Combust Flame 2017;179:172–84. https://doi.org/10.1016/j.combustflame.2017.01.018.
[30] Melder J, Zinsmeister J, Grein T, Jürgens S, Köhler M, Oßwald P. Comprehensive two-dimensional gas chromatography: a universal method for composition-based prediction of emission characteristics of complex fuels. Energy Fuels 2023;37(6):4580–95. https://doi.org/10.1021/acs.energyfuels.2c04270.
[31] Romanczyk M. Chemical compositional analysis of jet fuels: contributions of mass spectrometry in the 21st century. Mass Spectrom Rev 2024;43(2):345–68. https://doi.org/10.1002/mas.21825.
[32] Shi X, Li H, Song Z, Zhang X, Liu G. Quantitative composition-property relationship of aviation hydrocarbon fuel based on comprehensive two-dimensional gas chromatography with mass spectrometry and flame ionization detector. Fuel 2017;200:395–406. https://doi.org/10.1016/j.fuel.2017.03.073.
[33] Vozka P, Modereger BA, Park AC, Zhang WTJ, Trice RW, Kenttämaa HI, et al. Jet fuel density via GC×GC-FID. Fuel 2019;235:1052–60. https://doi.org/10.1016/j.fuel.2018.08.110.
[34] Pütz F, Lüdtke H, Ramirez Hernandez A, Oßwald P, Le Clercq P, Bauder U, et al. Influence of branching degree-derived iso-alkane GC×GC subgroups on fuel property prediction. Energy Fuel 2025;39(37):18001–12. https://doi.org/10.1021/acs.energyfuels.5c02762.
[35] Kathrotia T, Oßwald P, Köhler M, Slavinskaya N, Riedel U. Experimental and mechanistic investigation of benzene formation during atmospheric pressure flow reactor oxidation of n-hexane, n-nonane, and n-dodecane below 1200 K. Combust Flame 2018;194:426–38. https://doi.org/10.1016/j.combustflame.2018.05.027.
[36] Kathrotia T, Oßwald P, Zinsmeister J, Methling T, Köhler M. Combustion kinetics of alternative jet fuels, Part-III: Fuel modeling and surrogate strategy. Fuel 2021;302:120737. https://doi.org/10.1016/j.fuel.2021.120737.
[37] Schripp T, Grein T, Zinsmeister J, Oßwald P, Köhler M, Müller-Langer F, et al. Technical application of a ternary alternative jet fuel blend – chemical characterization and impact on jet engine particle emission. Fuel 2021;288:119606. https://doi.org/10.1016/j.fuel.2020.119606.
[38] Wei Y, Kuanibieke J, Jin H. Experimental study of diphenylmethane gasification with supercritical CO2. Fuel 2024;367:131524. https://doi.org/10.1016/j.fuel.2024.131524.